Available online at www.sciencedirect.com
SCIENCE DIRECT®
Chemical Physics 305 (2004) 197–211
Chemical Physics
www.elsevier.com/locate/chemphys

A temperature-dependent Hartree approach for excess proton transport in hydrogen-bonded chains

R.I. Cukier *

Department of Chemistry, Michigan State University, East Lansing, MI 48824-1322, USA

Received 17 May 2004; accepted 25 June 2004
Available online 27 July 2004

Abstract

We develop a temperature-dependent Hartree (TeDH) approach to solving the N-dimensional Schrödinger equation, based on the time-dependent Hartree (TDH) approximation. The goal is to describe the dynamics of protonated hydrogen-bonded water chains in condensed phases, where the medium fluctuations drive the proton transfer. An adiabatic simulation method (ASM) that couples the TeDH wavefunction to classical molecular dynamics (MD) propagation is used to obtain the real-time dynamics of the quantum protons that interact with the nuclear degrees of freedom. Iteration of the TeDH-ASM provides a trajectory from which the quantum dynamics of the protonated chains can be obtained. The method is applied to proton transfer in cytochrome *c* oxidase (CcO), which has a glutamate residue whose carboxylate may become protonated, as part of the mechanism of proton translocation. By using MD, we find that this glutamate can be hydrogen bonded to two water molecules in a cyclic structure. Application of the TeDH-ASM shows that a proton can transfer from one of the hydrogen-bonded waters to protonate this glutamate.

Keywords: Proton transfer and translocation; Cytochrome *c* oxidase

1. Introduction

The membrane-bound proteins active in photosynthesis and respiration have optimized structures that utilize energy gathered along a charge-separating network to drive a proton pump, which results in a transmembrane chemical potential that provides the energy for the synthesis of complex biomolecules [1]. A common theme in these exquisitely engineered systems is the possibility of rapid translocation of protons. One mechanism for proton translocation is via chains of hydrogen-bonded waters, using a "proton wire" concept [2] that has its origin in the Grotthuss [3] mechanism. The speed is attributed to an excess proton "hopping" along the water chain by a series of making and breaking hydrogen bonds, which does not require the slow process of molecular diffusion. Membrane-spanning water chains of varying lengths are found in a number of systems, including bacteriorhodopsin [4] and the photosynthetic reaction center of *Rhodobacter sphaeroides* [5,6]. Internal waters in conjunction with titratable amino-acid residues are thought to be responsible for proton uptake in cytochrome *c* oxidase (CcO), a membrane-bound enzyme that catalyzes the reduction of oxygen to water while producing an electrochemical gradient across the membrane in the form of a proton gradient [7–9].

Proton translocation in proteins introduces similar issues to the generic problem of a reactive region that one wants to treat by quantum mechanics coupled to a large

* Tel.: +5173559715; fax: +5173531793.
E-mail address: cukier@cem.msu.edu.

0301-0104/$ - see front matter © 2004 Elsevier B.V. All rights reserved.
doi:10.1016/j.chemphys.2004.06.060

system that can be treated classically. In the context of proton transfer, a great number of approaches to mixed quantum/classical treatments of single and multiple proton-transfer reactions have appeared [10–35]. For multiple proton transfers, there are Feynman path integral-based methods that are limited to equilibrium properties and use transition-state theory to obtain dynamical information [12,36–38], or use centroid molecular dynamics to probe dynamics [39–42]. Another general approach, when there are multiple quantum degrees of freedom coupled to classical degrees of freedom, relies on SCF and multi-configuration SCF methods to characterize real-time dynamics [43–49]. Closest in spirit, yet distinct from the work presented herein, are the simulations of proton chains by Pomès and Roux [38,50] and Hammes-Schiffer and coworkers [16,51–54]. Another approach that has been applied to bulk water [55,56], protonated water [57,58], ion channels [59], and model proton wires [60] is ab initio (Carr–Parrinello) [61] molecular dynamics (CPMD). To incorporate nuclear quantum effects from, e.g., protons [60,62], the nuclei can be quantized with use of the Feynman path integral method [63], (a PI-CPMD method). The PI-CPMD method is limited to equilibrium properties and is computationally demanding.

In this paper, we develop a methodology that combines a quantum mechanical treatment of the transferring protons with molecular dynamics (MD) for advancing the classically treated degrees of freedom, which is capable of describing the real-time dynamics of proton translocation in hydrogen-bonded chains, and apply it to CcO. By adiabatically separating the protons to be treated quantum mechanically from the other degrees of freedom, an adiabatic simulation method (ASM) that was previously used to discuss the properties of an excess electron in liquids [64–68] can be introduced. The quantum "active" protons' wave function is evaluated parametrically on the nuclear configuration of the rest of the chain and the surrounding medium. The nuclear configuration is then updated by, e.g., MD, where the time scale for the MD step is the nuclear time scale. The forces for the MD step are obtained from the sum of the classical medium/heavy-atom chain potential energy and the quantum force that the active protons exert on the nuclear degrees of freedom. The above procedure is iterated for a sufficient MD time interval to extract the desired information. The approach we develop does rely on the assumption that the active protons are always in their ground-state configuration; thus, contributions from excited states to the dynamics of the chain are neglected.

To apply the ASM to a proton chain is straightforward in principle but, for a chain with N quantum protons, becomes computationally intensive. Various SCF methods [43–48,69–71], have been used to reduce the poor scaling in N that exact methods would entail. One class of approximation is the time-dependent Hartree (TDH) approximation [72,73]. We formulate a version of this method that we will refer to as a *temperature*-dependent Hartree (TeDH) approximation. Validation of the method is explored by comparison of its predictions with numerically-exact solutions. Good agreement is found between the TeDH solutions and the numerically exact solutions, providing confidence in the methodology.

To apply the TeDH-ASM to proton translocation in CcO, we must first find hydrogen-bonded chains of waters and, possibly, residues. MD simulations that we have carried out [74,75] show that two water molecules become hydrogen bonded to a glutamate's (Glu286) carboxylate oxygens and that the waters are hydrogen bonded to each other. This hydrogen-bonded "cyclic" structure of two waters and the carboxylate oxygens is quite persistent in time. An excess proton is then added to one of the waters, and the possibility of proton transfer between the waters, and between one of the waters and one of the glutamate oxygens correlated with the water–water proton transfer, is investigated. The protons do rapidly "hop" between their respective heavy atoms. The proton that is between a water and a carboxylate oxygen can spend comparable time covalently bonded to the water and to the carboxylate, lending support to the hypothesis of a protonated Glu286 [40,76–78].

The plan of the remainder of this paper follows: In Section 2, the TeDH approximation is formulated and we introduce a solution method based on the symmetric split-operator propagation scheme [79–82]. We show that the method can be extended to apply to the TeDH equations where the Hamiltonian is now a temperature-dependent operator. In Section 3, we show that the TeDH equations do provide an accurate solution of the many active proton problems by comparing the TeDH solutions with those obtained by numerically exact two- and three-dimensional solutions for model two and three active proton chains whose potential function for the two active proton chain is a fit to ab initio-derived data. The MD program to simulate CcO is introduced in Section 4 and the results of the TeDH-ASM are given. Section 5 presents our concluding remarks.

2. A temperature-dependent Hartree (TeDH) approximation

A rationale for why a TDH or TeDH scheme should be reasonable for the proton-chain application can be stated in general terms [71]. Consider, for simplicity, but without loss of generality, two quantum protons. If the wavefunctions $\psi_i(x_i)$ $(i = 1,2)$ of the protons are

localized initially between their respective flanking groups, and if over some time interval they remain localized, then a semiclassical approximation is warranted. The bonding of the protons will, of course, prevent the protons from delocalizing away from their respective flanking groups. Then, the potential felt by, e.g., proton one is very nearly the potential due to a classical particle with position $x_2(t) = \langle\psi_2(x_2,t)|x_2|\psi_2(x_2,t)\rangle$ interacting with proton one via the potential $V(x_1,x_2(t))$. Hence, $\langle\psi_2(x_2,t)|V(x_1,x_2)|\psi_2(x_2,t)\rangle \approx V(x_1,x_2(t))$ will be a better approximation the more classical the particles. In other words, because the protons are well localized between their flanking groups, they are reasonably suited to a SCF scheme that uses mean-field potentials, $V(x_1,x_2(t))$.

The time-dependent Schrödinger equation with the replacement $t = -\mathrm{i}\beta\hbar$ is

$$-\frac{\partial\Psi}{\partial\beta} = H\Psi, \tag{2.1a}$$

where $H = H_0 + V$, with

$$H_0 = \sum_i (T_i(x_i) + V_i(x_i)) \equiv \sum_i H_i(x_i) \tag{2.1b}$$

and

$$V = \sum_{i<}\sum_{j} V_{ij}(x_i x_j) + \sum_{i<}\sum_{j<}\sum_{k} V_{ijk}(x_i x_j x_k). \tag{2.1c}$$

We have decomposed the total potential for the degrees of freedom that we shall treat quantum mechanically (the "active" protons) in terms of one-, two-, and three-body contributions. This decomposition should be sufficient to approximately characterize ab initio-based potential surfaces for the active protons. If a greater range of correlation is required, appropriate terms may be added onto the decomposition of Eq. (2.1c). The errors of the approach then will be controlled by the ability to fit these potential surfaces to suitably parameterized functions and, of course, limited by the accuracy of the TeDH methodology.

The temperature-dependent Hartree equations of motion are obtained by writing $\Psi = \prod_i \psi_i(x_i,\beta)$ and multiplying the Schrödinger equation by $\int \mathrm{d}x_1,\ldots,\mathrm{d}x_{i-1}\,\mathrm{d}x_{i+1},\ldots,\mathrm{d}x_N \prod_{j\neq i}\psi_j(x_j,\beta)$ to obtain (we use real wavefunctions throughout, as appropriate to the solution of Eq. (2.1))

$$-\partial\psi_i(x_i,\beta)/\partial\beta = \big(H_i(x_i) + \mu^i(\beta) + \langle V\rangle_i(\beta) + \bar{V}_i(x_i,\beta)\big)\psi_i(x_i,\beta). \tag{2.2}$$

The terms on the right-hand side of Eq. (2.2) have the following meanings: The one-body contributions to Eq. (2.2) pass through unchanged from Eq. (2.1b), of course. Let us define β-dependent normalization constants $N_i^2(\beta)$ that will be important to the proper formulation of a TeDH approximation, along with energies $\varepsilon_i(\beta)$ and $\gamma_i(\beta)$, and the convenient definitions of $\mu_i(\beta)$ and $\mu^i(\beta)$ as:

$$\begin{aligned}
N_i^2(\beta) &\equiv \int \mathrm{d}x_i \psi_i(x_i,\beta)\psi_i(x_i,\beta),\\
\varepsilon_i(\beta) &\equiv \int \mathrm{d}x_i \psi_i(x_i,\beta)\partial\psi_i(x_i,\beta)/\partial\beta/N_i^2(\beta),\\
\gamma_i(\beta) &\equiv \int \mathrm{d}x_i \psi_i(x_i,\beta)H_i(x_i)\psi_i(x_i,\beta)/N_i^2(\beta),\\
\mu_i(\beta) &\equiv \varepsilon_i(\beta) + \gamma_i(\beta) \text{ and } \mu^i(\beta) = \sum_{k\neq i}\mu_k(\beta).
\end{aligned} \tag{2.3}$$

The two- and three-body potentials contribute a term $\langle V_i\rangle(\beta)$ that is defined by the expectation values

$$\begin{aligned}
\langle V_i\rangle(\beta) &\equiv \sum_{j\neq i}\sum_{<k\neq i}\langle V_{jk}\rangle(\beta) + \sum_{j\neq i}\sum_{<k\neq i}\sum_{<\ell\neq i}\langle V_{jk\ell}\rangle(\beta),\\
\langle V_{jk}\rangle(\beta) &\equiv \int \mathrm{d}x_j\mathrm{d}x_k\psi_j(x_j,\beta)\psi_k(x_k,\beta)V_{jk}(x_jx_k)\psi_j(x_j,\beta)\psi_k\\
&\quad\times(x_k,\beta)/N_j^2N_k^2,\\
\langle V_{jk\ell}\rangle(\beta) &\equiv \int \mathrm{d}_j\mathrm{d}x_k\mathrm{d}x_\ell\psi_j(x_j,\beta)\psi_k(x_k,\beta)\psi_\ell(x_\ell,\beta)\\
&\quad\times V_{jk\ell}(x_jx_kx_\ell)\psi_j(x_j,\beta)\psi_k(x_k,\beta)\psi_\ell(x_\ell,\beta)/N_j^2N_k^2N_\ell^2.
\end{aligned} \tag{2.4}$$

The last term is the temperature- and coordinate-dependent one:

$$\bar{V}_i(x_i,\beta) = \sum_{j\neq i}\bar{V}_{i,j}(x_i,\beta) + \sum_{j\neq i}\sum_{<k\neq i}V_{i,jk}(x_i,\beta), \tag{2.5a}$$

where

$$\begin{aligned}
\bar{V}_{i,j}(x_i,\beta) &\equiv \int \mathrm{d}x_j\psi_j(x_j,\beta)V_{ij}(x_ix_j)\psi_j(x_j,\beta)/N_j^2(\beta),\\
\bar{V}_{i,jk}(x_i,\beta) &\equiv \int \mathrm{d}x_j\mathrm{d}x_k\psi_j(x_j,\beta)\psi_k(x_k,\beta)V_{ijk}(x_ix_jx_k)\psi_j\\
&\quad\times(x_j,\beta)\psi_k(x_k,\beta)/N_j^2(\beta)N_k^2(\beta).
\end{aligned} \tag{2.5b}$$

An interesting identity can be obtained by multiplying Eq. (2.2) by ψ_i and integrating over x_i:

$$\sum_i(\varepsilon_i + \gamma_i) = -\sum_i\langle V\rangle_i \equiv -\langle V\rangle. \tag{2.6}$$

For the purposes of the TeDH, we have not found this identity to be particularly useful, as is the case for the analogous one in the time-dependent Hartree theory [70]. Now, define

$$\varphi_i(x_i,\beta) = \mathrm{e}^{-\int^\beta\left(\mu^i(\beta')+\langle V\rangle_i(\beta')\mathrm{d}\beta'\right)}\psi_i(x_i,\beta). \tag{2.7}$$

Then, Eq. (2.2) may be written as

$$\partial\varphi_i(x_i,\beta)/\partial\beta = (H_i(x_i) + \bar{V}_i(x_i,\beta))\varphi_i(x_i,\beta) \tag{2.8}$$

and

$$\Psi = \mathrm{e}^{\sum_i\int^\beta\left(\mu^i(\beta')+\langle V\rangle_i(\beta')\mathrm{d}\beta'\right)}\prod_i\varphi_i(x_i,\beta). \tag{2.9}$$

The right-hand side of Eq. (2.9) is the TeDH approximation to Ψ. The wavefunctions $\varphi_i(x_i,\beta)$ obtained from Eq. (2.7) are sufficient to construct Ψ, as we will always normalize the wavefunction. This means that, at each step

in the quench (the solution of Eq. (2.8) as an initial value problem starting from $\beta = 0$ and terminating at some sufficiently large β value), the quantities

$$\bar{V}_{i,j}(x_i,\beta) = \int \mathrm{d}x_j \psi_j(x_j,\beta) V_{ij}(x_i x_j) \psi_j(x_j,\beta)/N_j^2 \equiv \int \mathrm{d}x_j \bar{\psi}_j(x_j,\beta) V_{ij}(x_i x_j) \bar{\psi}_j(x_j,\beta) \tag{2.10a}$$

and

$$\bar{V}_{i,jk} = \int \mathrm{d}x_j \mathrm{d}x_k \psi_j(x_j,\beta)\psi_k(x_k,\beta) V_{ijk}(x_i x_j x_k) \times \psi_j(x_j,\beta)\psi_k(x_j,\beta)/N_j^2 N_k^2 = \int \mathrm{d}x_j \mathrm{d}x_k \bar{\psi}_j(x_j,\beta)\bar{\psi}_k(x_k,\beta) V_{ijk}(x_i x_j x_k) \bar{\psi}_j(x_j,\beta) \times \psi_k(x_j,\beta)\bar{\psi}_k(x_k,\beta) \tag{2.10b}$$

are to be evaluated, where $\bar{\psi}_j(x_j,\beta)$ denotes the normalized version of $\psi_j(x_j,\beta)$. Because $\psi_j(x_j,\beta)$ and $\varphi_j(x_j,\beta)$ differ by just a β-dependent quantity according to Eq. (2.7), normalization ensures that we only need to solve the $\varphi_i(x_i,\beta)$ equations of Eq. (2.8). The solutions of the β-Schrödinger equation lead to real wavefunctions, assuming a real initial ($\beta = 0$) trial wavefunction.

The formal solution of Eq. (2.1) using a basis set $\{\phi_n(x^N)\}$ ($x^N = (x_1, x_2, \ldots, x_N)$) is

$$\Psi(x^N,\beta) = \sum_{n=0} a_n \mathrm{e}^{-\beta E_n} \phi_n(x^N) \tag{2.11}$$

and, for $\beta(E_1 - E_0) \gg 1$,

$$\Psi(x^N,\beta) \approx a_0 \mathrm{e}^{-\beta E_0} \phi_0(x^N). \tag{2.12}$$

The normalized ground-state wavefunction, $\bar{\phi}_0(x^N)$, then is obtained by normalizing the numerically obtained $\Psi(x^N,\beta)$ in Eq. (2.12). The method we use to solve the Schrödinger equation is based on the symmetrically split-operator, fast Fourier transform (FFT) technique developed by Feit et al. [79–82]. Using this method, the solution of Eq. (2.1) proceeds by propagating the Hamiltonian over some small $\Delta\beta$ step and accumulating enough steps to insure $\beta(E_1 - E_0) \gg 1$. A more efficient procedure [66,67], that we shall refer to as a "*decimation*" quench, starts with a relatively large $\Delta\beta$ and tests convergence of the energy (the expectation value of H) to some tolerance. Then, $\Delta\beta$ is halved and the same procedure of quenching and energy convergence is iterated until $\Delta\beta$ is less than some small quantity.

Applying an analogous method to the TeDH-approximated equations in Eq. (2.8) requires some development. Because wavefunctions contribute to the Hamiltonian via the $\bar{V}_i(x_i,\beta)$ terms, a propagation algorithm that accounts for a β-dependent Hamiltonian has to be used. The formal solution of Eq. (2.8) involves a β-ordered exponential operator as $[\hat{H}(\beta_1), \hat{H}(\beta_2)] \neq 0$ for $\beta_1 \neq \beta_2$. Of concern, too, is the order of the error term of the method. The symmetric split-operator method for a β-independent Hamiltonian is accurate to $O(\Delta\beta)^3$ [79,82]. In Appendix A we show that, for a Hamiltonian $\hat{H}(x,\beta) = \hat{T}(x) + V_0(x) + \bar{V}(x,\beta)$, the one-step propagator:

$$\psi(x,\beta_0 + \Delta\beta) \approx \mathrm{e}^{-\hat{H}(x,\beta_0)\Delta\beta}\psi(x,\beta_0) \approx \mathrm{e}^{-\hat{T}(x)\Delta\beta/2}\mathrm{e}^{-(V_0(x)+\bar{V}(x,\beta_0))\Delta\beta}\mathrm{e}^{-\hat{T}(x)\Delta\beta/2}\psi(x,\beta_0) + O(\Delta\beta)^3 \tag{2.13}$$

has, as indicated, the same order of error as the usual method. Therefore, in principal, application of a quench method of solution to the TeDH equations should also be an efficient method of solution of Eq. (2.8).

The issue arises of how to carry out the quench with regard to the convergence to the ground state. There no longer is a formal eigenvalue–eigenvector decomposition, as in Eq. (2.11), for the β-dependent Hamiltonian to provide guidance. The situation is similar to "SCF" problems that are solved with a basis set by using a trial wavefunction where matrix elements of the Hamiltonian depend on the wavefunction. There, iteration between the trial wavefunction and the Schrödinger equation is carried out until convergence is achieved. We will apply the quench method as described above and use Eq. (2.13) for the propagation. The solutions of Eq. (2.8) for all the degrees of freedom are simultaneously advanced over a $\Delta\beta$ interval, since all the wavefunctions are required to construct the $\bar{V}_i(x_i,\beta)$. A choice must be made regarding an "energy" test. The simplest procedure is to use the total (sum over all degrees of freedom) expectation value of the Hamiltonian. To summarize, we solve the TeDH equations of Eq. (2.8) using repeated application of the propagator in Eq. (2.13) with use of the decimation-quench method based on the expectation value of the Hamiltonian. As shown in the next Section, using this method leads to reliable results.

3. TeDH procedure validation

The accuracy of the TeDH method can be assessed by comparison either with analytic solutions or numerically exact solutions for the wavefunctions arising from two- (or higher) dimensional Hamiltonians. It is possible to demonstrate the accuracy of the method on an analytically solvable quadratic form Hamiltonian but it is not of sufficient complexity to be convincing in a general context. Thus, we instead consider models of proton chains with two and three active protons, and compare the TeDH-generated solutions with numerically exact solutions that are generated with a "conventional" quench method. That is, the two- (three-) dimensional Schrödinger equation is solved using the same Fourier transform methodology as in the TeDH discussed in

Section 2, using, of course, a 2D (3D) Fourier transform. The overhead associated with constructing the β-dependent potential energies $\bar{V}_i(x_i,\beta)$ at each step in the quench is gone, but it is certainly true that the TeDH is much faster than the numerically exact two- and three-dimensional calculations. We could detect no difference in quench efficiency between using the split-operator method with the β-dependent Hamiltonian required in the TeDH solution versus the split-operator method for a β-independent Hamiltonian. This indicates the correctness of the argument made in Appendix A showing that the split-operator method's error term is not increased by having to deal with a β-dependent Hamiltonian.

The coordinate system we adopt for the proton chain is shown in Fig. 1. The ith active proton's coordinate $r_{i\mathrm{H}}$ is referenced to the ith oxygen on its "left," as this permits ready expression of the notion that an excess proton is injected from the left side of a membrane and will exit from the other, "right," side of the membrane. Oxygen–oxygen distances are denoted as $r_{i,i+1}$ where $i=1$ denotes the left-most oxygen in the chain. When a specific oxygen pair, such as the one-two pair, is designated, we refer to its distance as r_{12}. Referencing the active proton distances, as defined above, will let us plot the respective wavefunctions on a common axis, as each proton's origin is on its left-side oxygen.

For $H_5O_2^+$, a "chain" with one active proton. Scheiner has fit the results of ab initio calculations of the active proton potential energy surface, parametric on the oxygen–oxygen distance r_{12} to various functional forms [83,84]. A Morse-based representation that works well is

$$V_{1\mathrm{H}}(r_{1\mathrm{H}}|r_{12}) = D\Big[\big(1-\mathrm{e}^{-\alpha(r_{1\mathrm{H}}-r_{1\mathrm{He}})}\big)^2+\big(1-\mathrm{e}^{-\alpha(-r_{1\mathrm{H}}-r_{1\mathrm{He}}+r_{12})}\big)^2 -\big(1-2\mathrm{e}^{2\alpha(r_{1\mathrm{He}}-r_{12})}\big)\Big], \tag{3.1}$$

where the last term serves to set the zero of energy of $V_{1\mathrm{H}}$ at the minimum-energy point(s) for the proton surface. The characteristic features of many hydrogen-bonded interfaces are found for this water cation; namely, a double-well form of the proton potential for larger r_{12} values, with a large barrier that rapidly drops as r_{12} decreases, yielding a single minimum potential surface for sufficiently short r_{12}. The Morse parameters of the potential are given in Table 1. For a chain $H_7O_3^+$ with two active protons, ab initio calculations were fit to the form

$$V_{\mathrm{TOT}} = V_{1\mathrm{H}}(r_{1\mathrm{H}}|r_{12}) + V_{2\mathrm{H}}(r_{2\mathrm{H}}|r_{23}) + V_{12}(r_{1\mathrm{H}},r_{2\mathrm{H}}|r_{12}), \tag{3.2}$$

where

$$V_{12} = -k(r_{1\mathrm{H}}-(r_{12}-r_{1\mathrm{He}}))(r_{2\mathrm{H}}-r_{2\mathrm{He}}). \tag{3.3}$$

This expression is the result of a fit with $r_{12}=r_{23}$; thus the lack of an explicit dependence on r_{23} in Eq. (3.3). The value of the interaction constant k is given in Table 1.

Table 1
Morse parameters in Eq. (3.1) and interaction constant in Eq. (3.3)

$r_{1\mathrm{He}}$ (Å)	α (Å^{-1})	D (kcal/mol)	k (kcal/mol)
0.97	2.68	76.0	65.0

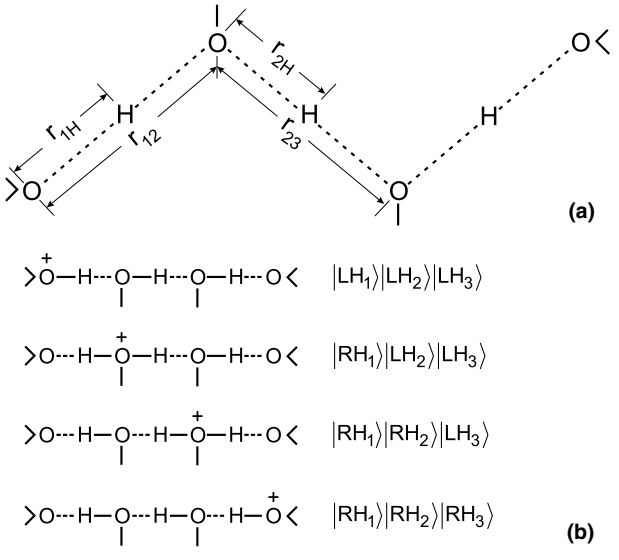

Fig. 1. (a) A proton chain $H_9O_4^+$ with one excess proton. The active protons' coordinates $r_{1\mathrm{H}},r_{2\mathrm{H}},\ldots$ are referenced to the oxygen atoms to their respective left, and the inter-oxygen distances are denoted as $r_{12},r_{23},\ldots$The excess proton can migrate from left to right by a "hopping" mechanism (cf. Section 1). (b) The proton ground-state locations are denoted as $|\mathrm{UH}_1\rangle|\mathrm{UH}_2\rangle|\mathrm{UH}_3\rangle$ with U denoting a left (L) or right (R) localized proton.

A contour plot of this V_{TOT} is shown in Fig. 2. The oxygen distances, $r_{12}=r_{23}=2.7$ Å, provide double minimum potential surfaces in the $r_{1\mathrm{H}}$ and $r_{2\mathrm{H}}$ coordinate directions, with barrier heights around 5 kcal/mol. The absolute minimum corresponds to proton 1 having transferred and proton 2 in its initial state, $|\mathrm{RH}_1\rangle|\mathrm{LH}_2\rangle$, assuming that both protons were initially "left" localized. The other two minima ($|\mathrm{LH}_1\rangle|\mathrm{LH}_2\rangle$ and $|\mathrm{RH}_1\rangle|\mathrm{RH}_2\rangle$) are of equal energy and are about 1.1 kcal/mol higher in energy than the true minimum. The interaction term, V_{12} strongly disfavors the doubly charged state $|\mathrm{LH}_1\rangle|\mathrm{RH}_2\rangle$, in accord with chemical principles. The harmonic proton frequency, $\omega_{1\mathrm{H}}$, based on expanding, e.g., $V_{1\mathrm{H}}(r_{1\mathrm{H}}|r_{12})$ around $r_{1\mathrm{He}}$ is $\omega_{1\mathrm{H}}\sim 3000$ cm^{-1}, implying a zero-point energy around 5 kcal/mol. In this situation, the solvation coming from the environment can provide a path for proton motion, where the first proton can transfer and then the second may transfer. As will be shown below, the protons are both localized around the absolute minimum for this potential surface. When the oxygen–oxygen distances are reduced to $r_{12}=r_{23}=2.4$ Å, the potential surface exhibits a single minimum, with no subsidiary minima. The one-dimensional surfaces

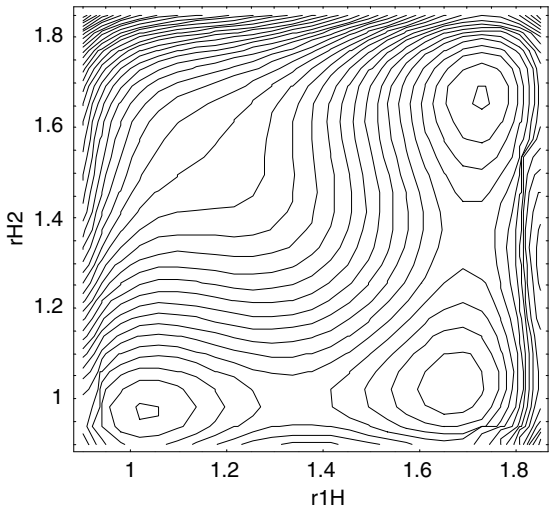

Fig. 2. Contour plot of V_{TOT} with the functional form in Eq. (3.2) and parameters given in Table 1, for $r_{12} = r_{23} = 2.7$ Å. The minimum of the potential is at $|RH_1\rangle\,|LH_2\rangle = (1.674,1.026)$ Å with energy 0.2265 kcal/mol. The two other subsidiary minima are $|LH_1\rangle|LH_2\rangle = (1.033,0.971)$ Å and $|RH_1\rangle|RH_2\rangle = (1.729,1.667)$ Å with energy 1.293 kcal/mol. There is a "path" for proton motion that, starting with both protons on the "left" ($r_{1H} \approx r_{2H} \approx 1.0$ Å), will first transfer proton one and then transfer proton two.

V_{1H} and V_{2H} also only have one minimum in accord with the short oxygen–oxygen distance. Again, the doubly charged state is strongly disfavored by the V_{12} term.

The above potential energy formulation can be applied to chains with more than two protons, by returning to the pair and triplet decomposition of the potential introduced in Eq. (2.1c). For the purposes of this work, we shall use just the pair terms, as the ab initio data has only been obtained for chains with two active protons. Of course, as more refined potential data becomes available, it will be straightforward to incorporate such three-proton correlations into the formalism.

3.1. Validation of the TeDH approximation on the two-proton chain

We shall consider several r_{12} and r_{23} distances to illustrate the accuracy and potential difficulties of the TeDH method. If there is a very large barrier along the r_{1H} and r_{2H} directions, it could be that a poor choice of initial wavefunction will not lead to the correct ground state for the TeDH method. If the wavefunction is "trapped" in a local minimum, it may not be able to tunnel out through a large barrier and find the true ground state. Note that, though, for large barriers the mechanism of proton transfer would no longer be dominated by the ground state; it would go over to a deep tunneling regime with a very different mechanism associated with a slow rate of transfer.

The protons' potential surface is displayed in Fig. 2 for $r_{12} = r_{23} = 2.7$ Å. The initial wavefunctions for the quenches of both protons are taken to be Gaussians; oscillator ground states with widths appropriate to a harmonic oscillator with frequency chosen as the local well frequency. The initial quench step is $\Delta\beta = 0.1$, the energy convergence condition is set to 0.0001 and $\Delta\beta$ is halved until $\Delta\beta < 0.01$. (These quantities are in dimensionless internal units of $\hbar\omega_{1H}/2$ where 1 unit $\sim$ 5 kcal/mol.) The notation for the wavefunctions is shown in Fig. 1(b), except for the designation $|SH_1\rangle|SH_2\rangle$. Here, the origin of each oscillator wavefunction is chosen half-way between the two equilibrium positions of the protons. This ensures a much better chance of converging to the correct ground state. (The units of energy in the table are internal units and the 0.127 energy difference is around 0.6 kcal/mol.)

Table 2 summarizes the results of the 2D and TeDH quenches. The ground state is found to be $|RH_1\rangle|LH_2\rangle$. The 2D results show that all the initial wavefunctions examined go to the correct ground state. The initial wavefunction denoted as $|L'H_1\rangle|LH_2\rangle$ ($|L''H_1\rangle|LH_2\rangle$) shifts the origin of proton one's wavefunction 0.1 Å to the right (left), relative to the $|LH_1\rangle|LH_2\rangle$ initial choice. The TeDH quench is not correct for the initial choices $|LH_1\rangle|LH_2\rangle$ and $|L''H_1\rangle|LH_2\rangle$, but moving the origin of proton one 0.1 Å to the right (the $|L'H_1\rangle|LH_2\rangle$ initial wavefunction) corrects this. Furthermore, if we slightly broaden the initial wavefunction from its harmonic oscillator width, in units scaled by the length $\ell = \sqrt{\hbar/m\omega}$, $\psi_1(x) \approx \exp(-x^2/2)$, to $\psi_1(x) \approx \exp(-0.8x^2/2)$, then the TeDH again predicts the correct ground state. It is important to note that while we report an "energy" in the TeDH method,

Table 2
Two active protons with $r_{12} = r_{23} = 2.7$ Å

Initial state	Two-dimensional		TeDH	
	Final state	Energy[a]	Final state	Energy
$\|LH_1\rangle\|LH_2\rangle$	$\|RH_1\rangle\|LH_2\rangle$	1.3828	$\|LH_1\rangle\|LH_2\rangle$	2.0001
$\|SH_1\rangle\|SH_2\rangle$	$\|RH_1\rangle\|LH_2\rangle$	1.3828	$\|RH_1\rangle\|LH_2\rangle$	1.5037
$\|RH_1\rangle\|LH_2\rangle$	$\|RH_1\rangle\|LH_2\rangle$	1.3828	$\|RH_1\rangle\|LH_2\rangle$	1.5037
$\|L'H_1\rangle\|LH_2\rangle$	$\|RH_1\rangle\|RH_2\rangle$	1.3828	$\|RH_1\rangle\|LH_2\rangle$	1.5037
$\|L''H_1\rangle\|LH_2\rangle$	$\|RH_1\rangle\|LH_2\rangle$	1.3828	$\|LH_1\rangle\|LH_2\rangle$	2.0004
$\|LH_1\rangle\|H_2\rangle$	$\|RH_1\rangle\|LH_2\rangle$	1.3828	$\|RH_1\rangle\|LH_2\rangle$	1.5037

[a] Energy is given in internal dimensionless units. The conversion to kcal/mol is effected by multiplying by 5.0 kcal/mol.

it is not an energy in the sense of an eigenstate. The TeDH (and TDH) methods cannot give eigenstate energies.

The individual proton probabilities are displayed in Fig. 3. As the probabilities will be used in evaluating the quantum forces for the MD evolution, it is important that the TeDH approximation represent them accurately, and it does. The probabilities displayed in Fig. 3 have much more weight toward the centers then the extremities of the surfaces. Therefore, as the exploration of different initial wavefunctions in Table 2 and our observation about using slightly wider initial choices indicates, the TeDH method should be capable of yielding the correct ground state when the wavefunctions from a previous MD configuration are used as the initial wavefunctions for the current configuration's quench.

When the oxygen–oxygen distances are short, e.g., $r_{12} = r_{23} = 2.4$ Å, single-well surfaces are obtained. There is only one minimum, in accord with the single-proton coordinate potential surfaces. Starting from initial states $|SH_1\rangle|SH_2\rangle$ or $|LH_1\rangle|LH_2\rangle$ for both 2D and TeDH methods lead to the same ground state. Both protons are shared between their respective flanking groups. For these short oxygen–oxygen distances where the ground state is unambiguous, any reasonable initial wavefunction will converge to the correct one, for both 2D and TeDH methods.

In the examples above, the oxygen–oxygen distances were set equal because these symmetric cases are the most demanding of the TeDH method. Naturally, proton chains with their heavy atom vibrational motion and coupling to a medium will not often have equal oxygen–oxygen distances. We have explored a number of cases where the r_{12} and r_{23} distances range from 2.4 to 2.7 Å and find that, in these asymmetric situations, the TeDH method gives essentially the exact results starting from the same initial wavefunctions as used for the exact quench method.

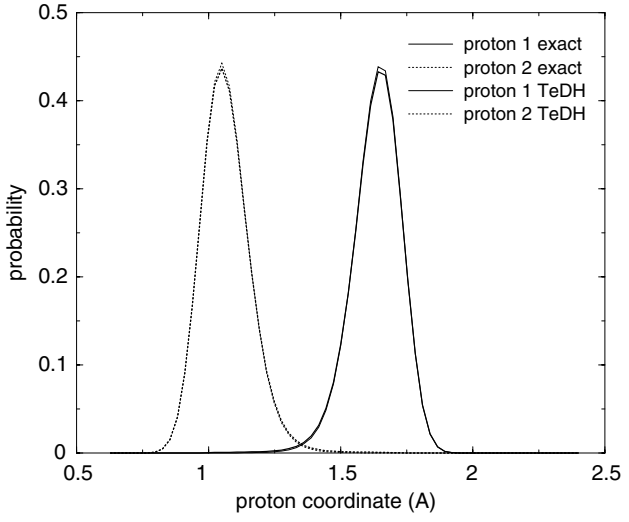

Fig. 3. Ground-state probabilities $\psi_i^2(r_{iH})$ $(i = 1,2)$ as predicted by the numerically exact 2D quench and the TeDH approximation. The oxygen–oxygen distances are $r_{12} = r_{23} =$ 2.7 Å. The TeDH approximation is clearly of excellent quality.

Finally, for $r_{12} = r_{23} = 3.0$ Å, there are large barriers (25 kcal/mol) along the r_{1H} and r_{2H} directions, suggesting that the initial condition of the quench method for the TeDH is crucial. Indeed, care must be exercised in the initial choice of wavefunction for the 2D quench also. Nevertheless, with suitable initial wavefunctions (they must be of the $|SH_1\rangle|SH_2\rangle$ type) both methods produce the correct ground state, even though the first excited state is extremely close in energy to the ground state.

3.2. Validation of the TeDH approximation on the three-proton chain

The potential surface for a three-active-proton chain with the assumption of only pair order terms in the potential is given by the first sum in Eq. (2.1c). We stress that the use of only pair order terms is a consequence of the available potential surface; it is not a limitation of the TeDH method. Note that the relative CPU time between the 3D and the TeDH methods is about a factor of 1200, when 64 points are used for the FFT grid. Even for a 3-proton chain, the numerically exact 3D method would not be feasible in the context of an MD simulation where the quench would have to be carried out for $\sim 10^6$ MD steps.

A new feature does arise in a three-proton chain that is not present for a two-proton chain. Examination of the potential surface for $r_{1H} = r_{12} - (r_{1He} - s)$ and $r_{3H} = r_{3He} + s$ as a function of r_{2H} yields a symmetric double well for proton two. This is evident from the symmetry of the chain when all oxygen–oxygen distances are the same; for a symmetric arrangement of protons one and three, relative to the chain's bisector, proton two will experience a symmetric potential. Indeed, using the above symmetry related coordinates for r_{1H} and r_{3H}, $V_{12} + V_{23} = -k(r_{12} - 2r_{1He})s$, showing that the summed correlation potential is a constant (with respect to r_{2H}) that depends on the value of s. The correlation parts cancel and, if the oxygen–oxygen distances are sufficiently large, the total potential will be a double well from the one-body V_2 term. It is then important that the initial wavefunction span the wells in order to converge to the correct ground state. In Table 3 we display the results of the numerically exact calculations for different initial conditions when there is a double well for proton two ($r_{12} = r_{23} = r_{34} = 2.7$ Å). The ground-state probabilities of the protons are shown is Fig. 4. Unless the initial wavefunctions are distributed over all the wells, $|SH_1\rangle|SH_2\rangle|SH_3\rangle$, or the initial wavefunctions are qualitatively the same as the corrects ones, $|RH_1\rangle|SH_2\rangle|LH_3\rangle$ (the second proton is distributed over the double well), then the wrong ground state will result.

Table 3
Three active protons with $r_{12} = r_{23} = r_{34} = 2.7$ Å

Initial state	Three-dimensional			TeDH		
	Final state[c,d]	Energy[a]	Iterations[b]	Final state[c,d]	Energy[a]	Iterations[b]
$\|LH_1\rangle\|LH_2\rangle\|LH_3\rangle$	$\|RH_1\rangle\|LsH_2\rangle\|LH_3\rangle$	2.5248	433	$\|RH_1\rangle\|SH_2\rangle\|LH_3\rangle$	2.9053	214
$\|SH_1\rangle\|SH_2\rangle\|SH_3\rangle$	$\|RH_1\rangle\|SPH_2\rangle\|LH_3\rangle$	2.5228	92	$\|RH_1\rangle\|SPH_2\rangle\|LH_3\rangle$	3.1567	118
$\|RH_1\rangle\|SH_2\rangle\|LH_3\rangle$	$\|RH_1\rangle\|SPH_2\rangle\|LH_3\rangle$	2.5228	77	$\|RH_1\rangle\|SPH_2\rangle\|LH_3\rangle$	3.1567	96
$\|LH_1\rangle\|SH_2\rangle\|LH_3\rangle$	$\|RH_1\rangle\|LsH_2\rangle\|LH_3\rangle$	2.5248	414	$\|RH_1\rangle\|SH_2\rangle\|LH_3\rangle$	2.9053	207
$\|RH_1\rangle\|LH_2\rangle\|LH_3\rangle$	$\|RH_1\rangle\|LsH_2\rangle\|LH_3\rangle$	2.5243	422	$\|RH_1\rangle\|SH_2\rangle\|LH_3\rangle$	2.9056	113

[a] Energy is given in internal dimensionless units. The conversion to kcal/mol is effected by multiplying by 5.0 kcal/mol.
[b] Number of iterations in the quench.
[c] Ls denotes that the initially left-localized probability has split to have about 15% of its probability in the right well.
[d] SP denotes that the probability is symmetrically split over both wells.

The corresponding results for the TeDH are also shown in Table 3. It has no difficulty in producing the split probability for proton two. The TeDH is still an accurate procedure, though now the differences between the exact and TeDH are evident.

For smaller oxygen–oxygen distances, around 2.5 Å and shorter, the double well for proton two, when protons one and three are symmetrically disposed, is essentially gone. Both the numerically exact and TeDH methods will converge to the ground state as shown in Fig. 5, and the initial wavefunction can be, e.g., left localized. That is, the initial state $|LH_1\rangle|LH_2\rangle|LH_3\rangle$ now does go to the correct ground state. Again, there is some difference between the probabilities in the 3D and TeDH methods. We would anticipate, for this easier case, where there are no double wells to contend with, that the agreement between 3D and TeDH approaches might be better. Unfortunately, we were not able to use a 128^3 grid for the 3D calculation, as the memory requirements were too large. However, the agreement certainly is sufficiently good to consider the method reliable. Note that the quantum force is an integral over the probability weighted by the solvent-proton potential, and integration will smooth out small errors in the probabilities.

To sum up, the TeDH method gives excellent agreement when compared with the numerically exact 2D and 3D calculations for what we view as the most difficult cases of symmetric potential surfaces. When the surfaces are asymmetric, with their well-localized protonic states, the TeDH method is expected to be at least as reliable. Naturally, when the quantum system is coupled to a fluctuating medium, the chance of obtaining symmetric solvation potentials is remote, and asymmetric surfaces will dominate.

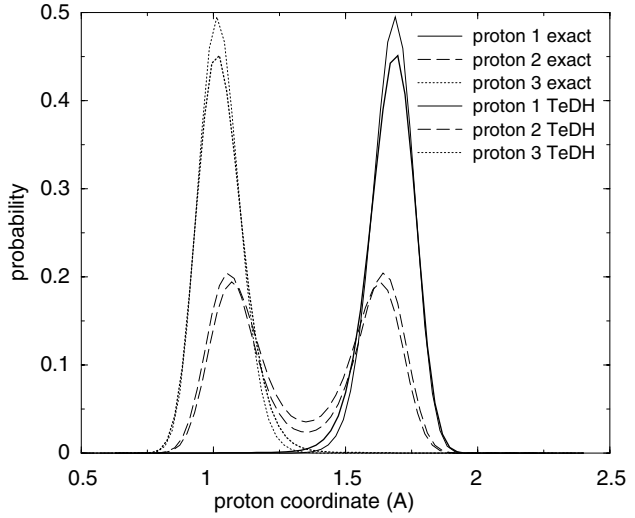

Fig. 4. Ground-state probabilities $\psi_i^2(r_{iH})$ $(i = 1–3)$ as predicted by the numerically exact 3D quench and the TeDH approximation. The oxygen–oxygen distances are $r_{12} = r_{23} = r_{34} = 2.7$ Å. The TeDH approximation is of good quality, though the difference with the exact result is evident. The second proton's wavefunction is symmetrically split, reflecting the cancellation of the two interaction terms when proton one and three are symmetrically disposed, with respect to the midpoint of the chain, and the oxygen–oxygen distance is sufficiently large that proton two's one-body potential is a (symmetric) double well (see the discussion in Section 3).

4. Temperature-dependent Hartree-adiabatic simulation method

4.1. Molecular dynamics

The molecular dynamics simulation is carried out using CUKMODY, a code designed for efficient simulation of proteins and other large solutes [85]. The GROMOS [86] force field is used for the residues and solvent water. A combination of a cell index method with linked lists [87] and a Verlet neighbor list [88] is used to provide linear scaling with the number of atoms in the pair list routine, essential for the large systems considered here. For the Verlet neighbor list, the outer distance is $r_l = 12.8$ Å and the inner distance is $r_c = 10.0$ Å. The update of the pair list is done whenever any atom moves a distance greater than $0.5(r_l - r_c)$, leading to updates roughly every 30 steps. The electrostatic interactions are evaluated using the charge-group method, to be consistent with the parameterization of the GROMOS force field. The SHAKE algorithm [89] is used to constrain bond lengths permitting a 2 fs

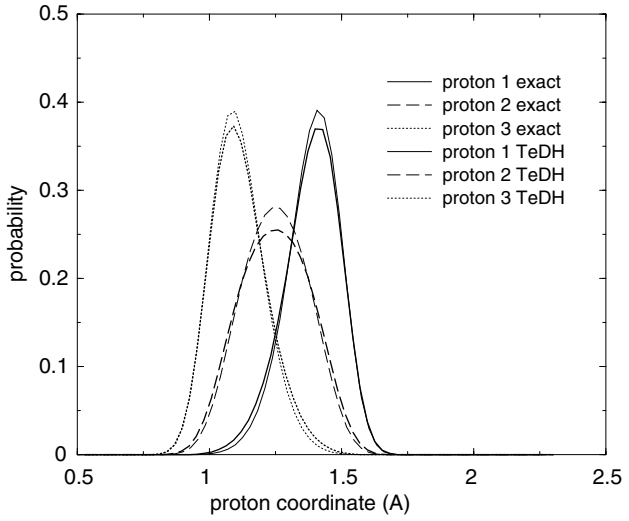

Fig. 5. Ground-state probabilities $\psi_i^2(r_{i\mathrm{H}})$ $(i = 1–3)$ as predicted by the numerically exact 3D quench and the TeDH approximation. The oxygen–oxygen distances are $r_{12} = r_{23} = r_{34} = 2.5$ Å. The TeDH approximation is of good quality, though the difference with the exact result is evident. The second proton is between its oxygens reflecting the cancellation of the two interaction terms when proton one and three are symmetrically disposed, with respect to the midpoint of the chain, and the oxygen–oxygen distance is sufficiently short that proton two's one-body potential is a single well (see the discussion in Section 3).

time step. Periodic boundary conditions are used. The simulation is carried out at constant NVT with velocity scaling [90] to control the temperature to around 300 K. The start-up protocol creates a face-centered cubic lattice of water molecules and centers the protein in the simulation cell. The waters that overlap the protein are discarded, based on their oxygen (atom O) to protein atom j distance $r_{\mathrm{O}j} < \sigma_{\mathrm{O}j}$, with $\sigma_{\mathrm{O}j}$ the van der Waals distance parameter. The simulation is started with the protein cold, and the solvent heats the protein as the solvent molecules equilibrate to each other and the protein.

The starting configuration was obtained from a preliminary version of the recently published X-ray crystal structure of cytochrome *c* oxidase from *Rhodobacter sphaeroides* [91]. Only subunits I and II were included in the simulation. The simulated protein had a total of 7705 atoms, including the polar hydrogens. Details of the force field, the protonation states of the residues, the charge assignments for the metals and the two type a heme cofactors are available in a previous study of CcO [75]. After removing overlapping waters, there were 18,399 water molecules left in the simulation box. The simulation box side is 88.7 Å, and the largest dimension of CcO is around 80 Å, leaving about 20 Å between protein molecules in neighboring cells. The large number of waters used facilitates investigation of the formation of hydrogen-bonded water structures.

The simulation of the protein/cofactors and waters was then initiated and periodically examined for configurations of waters that are hydrogen bonded together and to residues. Such clusters are tracked in time to find some that are relatively persistent. One such cluster that formed consisted of two waters and the residue Glu286. By convention, the glutamic acid residue is assumed to be deprotonated in the MD, thus a glutamate. The two waters hydrogen bond together, one (denoted as LW) hydrogen bonds to the OE2 carboxylate oxygen and the other (denoted as TW) to the OE1 carboxylate oxygen, as displayed in Fig. 6(a), 500 ps after startup. The alignment of the hydrogens, in their respective hydrogen bonds, are close to linear and the oxygen–oxygen atom distances are around 2.7 Å, indicating a stable hydrogen-bonding pattern. The cluster persists on the scale of hundreds of picoseconds, with the various heavy-atom, hydrogen-bonding distances undergoing small fluctuations. We will use this cluster to illustrate the TeDH-ASM.

4.2. Adiabatic simulation method

In the ASM [64–68], the atoms that are treated quantum mechanically exert a force on each "solvent" atom that has to be accounted for in the MD configuration update. The Hellmann–Feynman force [92,93] on the ith atom F_i^{qu} is defined as:

$$F_i^{\mathrm{qu}} = -\int \mathrm{d}\mathbf{x}^N \psi\left(\mathbf{x}^N;\mathbf{R}^N(t)\right)^2 \partial V\left(\mathbf{x}^N;\mathbf{R}^N(t)\right)/\partial \mathbf{R}_i, \quad (4.1)$$

where $V(\mathbf{x}^N;\mathbf{R}^N(t))$ is the sum of the gas-phase potential, introduced in Section 3 and the solvation component that depends parametrically on the classical atom coordinates $\mathbf{R}^N(t)$. (The proton coordinates are written as vectors here because, in the frame of the MD simulation box, they point in various directions.) The time dependence arises from the MD trajectory that depends in a self-consistent manner on the forces generated from both classical and quantum degrees of freedom. Given

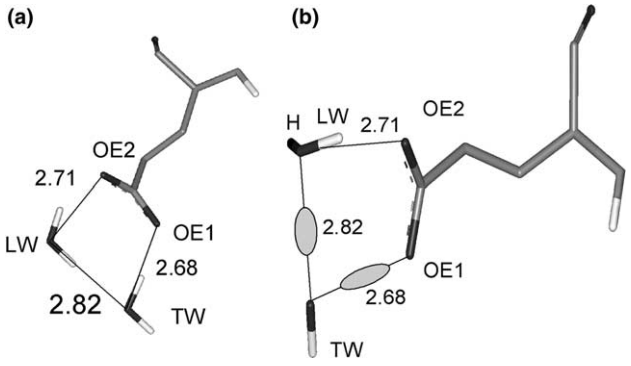

Fig. 6. (a) Two hydrogen-bonded waters, labeled TW and LW, which are hydrogen bonded to, respectively, the OE1 and the OE2 of the carboxylate group of Glu286. The geometry indicates that all three hydrogen bonds are strong. The structure is quite persistent in time. (b) A proton is added to the LW (it is the one pointing away from the LW oxygenOE2 hydrogen bond). The proton between LW and TW, and the proton between TW and OE1 are deleted, because they will be treated as active (quantum) protons.

a ground-state wavefunction $\psi(\mathbf{x}^N;\mathbf{R}^N(t))$ available from, e.g., the TeDH method, the quantum forces can be obtained from the current configuration. These forces along with the classical forces are used to update the system configuration by one MD step. The new configuration provides a new potential surface, a new TeDH wavefunction is computed and the scheme iterated.

4.3. Application to cytochrome c oxidase

The TeDH procedure in combination with the ASM can be used to assess the possibility of protonation of Glu286 by hydrogen-bonded waters. To make this definite, consider the waters labeled as LW and TW, and OE1 of Glu286, with an excess proton added to LW, as displayed in Fig. 6(b). The orientation of the added proton is defined by the geometry of the two waters. The two-active-proton species is then created by removing from the MD force field the hydrogen-bonded proton between the two waters and the hydrogen-bonded proton between TW and OE1. The two protons that were removed will be treated quantum mechanically, and are schematized as ovals in Fig. 6(b).

A potential surface for this system is not available directly; however, the pK_a of glutamic acid in various environments is known and tends to be increased, relative to its standard value of about 4.0, in protein active sites [94,95]. Indeed, there is spectroscopic evidence for protonation of Glu286 at neutral pH, with an estimated pK_a of 8–9 [40,76–78]. We carried out a high-level DFT ab initio quantum chemistry calculation [96] to obtain a gas phase surface for the cluster, with the glutamate anion replaced by an acetate anion. The heavy atom geometry of the cluster was fixed close to that from the simulation, and the other atom coordinates were relaxed to obtain a stable geometry. The potential surface for the two active protons was generated by scanning their respective positions in 0.1 Å increments. The configuration to form two waters and acetic acid (proton transferred to the carboxylate) is more stable than the ionized form by about 35 kcal/mol. Thus, the surface is quite strongly exoergic in favor of transferring a proton to the glutamate, relative to a system with the carboxylic acid replace by a water molecule, where the surface for the two active protons would be thermoneutral. This gas-phase surface does not account for stabilization by solvation of the charge-separated state. Thus, we will consider gas-phase surfaces that are close to thermoneutral.

The total potential energy surface for the active protons can be evaluated by moving the protons between their respective flanking oxygens and, for each proton position, evaluating the Coulomb interaction with the water, cofactor, and protein atom charges. There is "noise" on the scale of 1–2 kcal/mol in the solvation surface because, as the proton is moved, one or more surrounding atoms can move in or out of the cutoff sphere. Therefore, we have carried out a moving average over 3 neighboring points to construct the solvation surface. Most of the solvation comes from the protein, though there are a number of relatively close-by waters that also contribute.

Note that for an assumed symmetric surface, without solvation, the two-proton surface leads to a $|R\rangle|L\rangle$ ground state whereby there would be no proton transfer to the glutamate, as shown in Tables 2 and 3, for heavy-atom distances 2.7 and 3.0 Å. The solvation surfaces of the two active protons are displayed in Fig. 7 for the configuration just after creating the protonated species. These surfaces do *not* represent the true surface; this requires the correlation term in Eq. (3.3) and should be displayed as a two-dimensional surface. We plot these one-dimensional surfaces just to show how solvation affects the proton surfaces for two active protons. This solvation would favor the first proton to not transfer and the second one to transfer, a $|L\rangle|R\rangle$ state. However, the TeDH solution (and the numerically exact 2D FFT solution) shows that the ground state is still $|R\rangle|L\rangle$. The correlation term in Eq. (3.3) strongly disfavors the $|L\rangle|R\rangle$ state, as is evident from the contour map displayed in Fig. 2. The states $|R\rangle|R\rangle$ and $|L\rangle|L\rangle$ are energetically close to the $|R\rangle|L\rangle$ state, and we should anticipate that solvation will permit substantial population of these states, in addition to the $|R\rangle|L\rangle$ state.

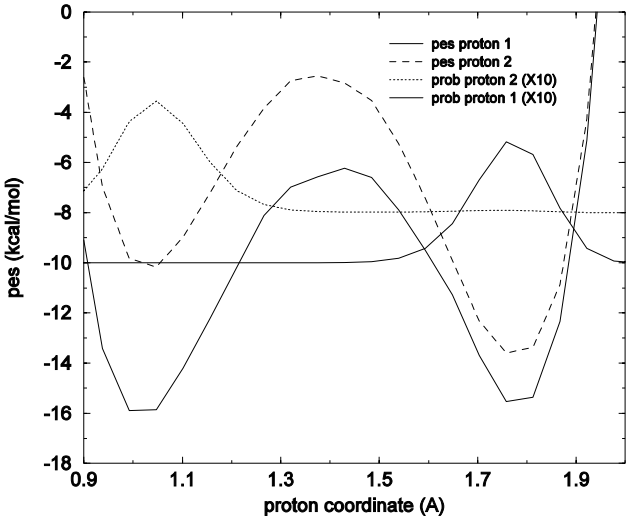

Fig. 7. The initial state (after adding the excess proton) solvated potential energy surfaces for moving one proton (labeled as proton 1) between the LW and the TW and another proton (labeled as proton 2) between the TW and the OE1 of Glu286 (cf. Fig. 6(b)). The proton probabilities are displayed multiplied by 10 to show up on the scale of the potential energy surface. The solvation slightly favors proton one to be on the left and strongly favors proton two to be on the right. The complete surface includes the proton–proton coupling (cf. Eq. (3.3)) and, as the wavefunctions show (cf. Table 2), the true ground state ($|R\rangle|L\rangle$) is the same as was found without solvation.

Fig. 8 displays the expectation value of each proton's position for the intervals 40–60 and 80–100 ps in a 100 ps run with $r_{12} = r_{23} = 2.8$ Å with the gas-phase contribution assumed to be symmetric (thermoneutral). The data for the remaining time is similar in character. The second proton's $\langle x\rangle(t)$ is displaced by 1 Å, for clarity of presentation. Both protons do quantum mechanically transfer on a femtosecond time scale. In particular, the second proton does transfer, indicating that Glu286 can be protonated by proton transfer from the water hydrogen bonded to it. Solvation can tip the gas-phase surface sufficiently to provide stable states corresponding to the second proton transferred. The solvation bandwidth, found by making a histogram of the differences in energy between the wells of the solvation surface over the trajectory, is around 5 kcal/mol. The proton jumps occur on a several femtosecond time scale since it does not take much rearrangement of the surroundings to provide a surface that tips from one side to another on the scale of kcal/mol.

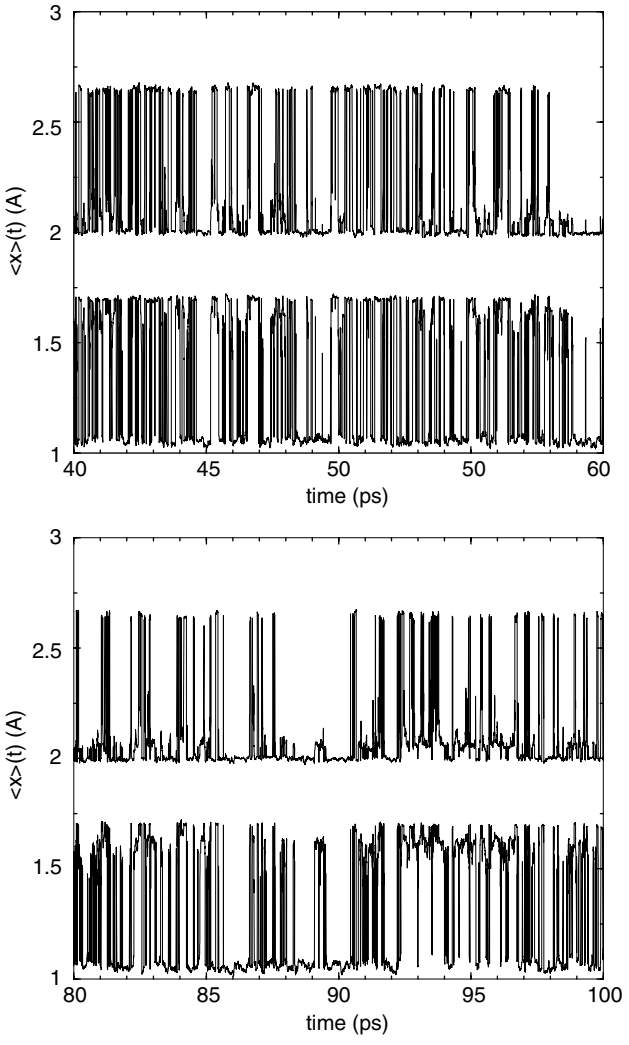

Fig. 8. The time-dependent expectation value $\langle x\rangle(t)$ of each proton's position with a symmetric gas-phase surface for the second proton. The data for proton 2 is displaced by +1 Å for clarity of presentation. The data for the intervals between 40–60 and 80–100 ps are displayed from a run of 100 ps. The second proton's $\langle x\rangle(t)$ indicates protonation of Glu286's OE1.

A free energy difference ΔG and corresponding equilibrium constant K_{eq} for each proton can be obtained from the fraction of time each proton spends in its two states. That is an advantage of the quantum mechanical treatment of the protons used here. The first proton (the one between the two waters) spends essentially equal time in each state, so its $K_{eq} \approx 1$. For the second proton (the one between the TW and the OE1) $K_{eq} \approx 0.27$ leading to a $\Delta G \approx 0.7$ kcal/mol, a modestly endothermic protonation process. A qualitative analysis of Fig. 8 shows that the protons are definitely correlated, as implied by the gas-phase potential energy surface. The states $|R\rangle|R\rangle$, $|R\rangle|L\rangle$ and $|L\rangle|L\rangle$ are by far the most prevalent. States with $|L\rangle|R\rangle$ are highly disfavored, though some do occur. There are some MD steps where $\langle x\rangle(t)$ is in the middle, i.e., the wavefunction is split between the two wells, but these are very rare. They might be states where a non-adiabatic transfer mechanism would be appropriate but clearly the adiabatic mechanism is dominant in these simulations, as anticipated.

To assess the role of an asymmetric gas-phase surface on the extent of Glu286 protonation, asymmetry was introduced in Eq. (3.1) by multiplying the second term by a scale factor, asym. For asym = 0.95, the one-dimensional surface for the second proton is ~2.5 kcal/mol endoergic (in the protonation direction). The 2D surface, for $r_{12} = r_{23} = 2.8$ Å, has the $|R\rangle|L\rangle$ state energy about 2.5 kcal/mol above the $|L\rangle|L\rangle$ and $|R\rangle|L\rangle$ states' energies. Fig. 9 displays the expectation values in a 100 ps run. From the length of time spent in each state, $K_{eq} = 0.09$ and $\Delta G = 1.44$ kcal/mol. For asym = 0.925, the one-dimensional surface for the second proton is ~5 kcal/mol endoergic. The 2D surface for $r_{12} = r_{23} = 2.8$ Å has stable wells with the $|L\rangle|L\rangle$ and $|R\rangle|L\rangle$ states approximately 5 kcal/mol lower in energy than the $|R\rangle|L\rangle$ well. The results from this run (data not shown) exhibit relatively few jumps (~1.7% of the total) to the protonated glutamate state. With this caution on the statistics, a 100 ps run leads to $\Delta G = 2.42$ kcal/mol. The solvation bandwidth of 5 kcal/mol can only rarely compensate for the 5 kcal/mol endoergic gas-phase surface to populate the $|R\rangle|L\rangle$ state. Conversely, if the TW-OE1 proton potential surface is made exoergic toward Glu286 protonation by a few kcal/mol, the Glu286 will be protonated most of the time [74,75].

5. Concluding remarks

In this work, we have formulated a temperature-dependent Hartree approximation for obtaining the ground-state solution of the N-dimensional Schrödinger

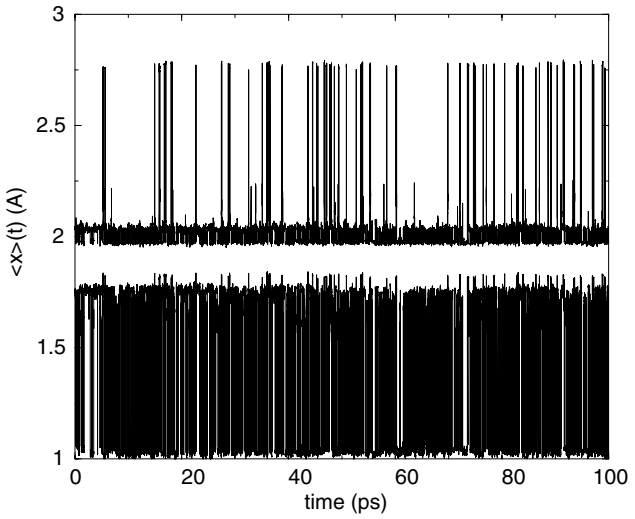

Fig. 9. The time-dependent expectation value $\langle x \rangle(t)$ of each proton's position. The second proton's gas-phase surface is endoergic by about 2.5 kcal/mol in the direction of Glu286 protonation. The data for proton 2 is displaced by +1 Å for clarity of presentation.

equation. The method was shown to be accurate for predicting the ground-state probabilities of up to three coupled protons by comparing the TeDH with the numerically exact FFT solutions. Because the TeDH method scales linearly with the number of quantum degrees of freedom, it is practical to treat problems with many coupled protons in schemes that require repeated solution for the quantum degrees of freedom. Once a ground-state wavefunction solution method is available, the ASM can be used to generate, by an iterative process between MD and QM, the real-time dynamics of the quantum-classical system. The TeDH-ASM must focus on ground states because *dynamics* based on a mixed quantum/classical evolution scheme, such as the adiabatic simulation method, is only correct for evolution in a definite state [64–68].

Fast proton-chain dynamics should be dominated by ground-state protons. Qualitatively, one may think of the overall process of proton transfer as a thermal average over the varying heavy-atom distances. The shorter distance configurations will have better quantum overlap of wavefunctions and lead to faster dynamics. Thus an adiabatic theory, appropriate to these shorter flanking atom distances, should be used to characterize fast proton-transport phenomena. Then, the crucial issue for obtaining a practical scheme for treating proton-chain dynamics is validation of the TeDH method, and this is what we have shown herein. Because a three-proton chain has contributions from both flanking protons of the middle proton in the TeDH scheme, validation of the TeDH at this level should then give confidence that it will also be accurate for longer chains. That is fortunate, as validation of the TeDH method by comparison with exact numerical solution of a four-proton chain would be computationally challenging.

Cytochrome *c* oxidase provides an ideal test bed for the TeDH-ASM because it presents a number of channels that are thought to support proton translocation through hydrogen-bonded water chains and residues. The MD simulation we carried out [74,75] shows that two waters form stable hydrogen bonds to Glu286, a residue that has been repeatedly implicated as contributing to proton translocation [76,91,97–103]. The results summarized by Figs. 8 and 9 support the possibility of proton dynamics on a fast time scale. A mechanism of proton motion by classical mass diffusion would lead to much slower dynamics. The protonation/deprotonation of Glu286's carboxylate oxygen is rapid because the solvation can easily "tip" the surface to favor one side or the other with a small rearrangement of the protons' surroundings. A utility of the TeDH-ASM is the direct interrogation of the fractional protonated population. Because the fraction is obtained from a time average over the fluctuations in the surroundings, relating it to an equilibrium constant and, consequently, a free energy is appropriate, at least if the average can be carried out for a sufficiently long time. It should be clear that the short time scale of the simulation may not be able to capture the solvating power of the protein.

There are a number of issues that should be addressed, to make our methods more efficient and more realistic for application to proton translocation in proteins that we now discuss. First, an analytic proof of the TeDH's correctness has not been obtained. Once the eigenvalue–eigenvector decomposition of the governing differential equations in Eq. (2.8) is no longer available, as it is for a temperature-independent Hamiltonian, (cf. Eqs. (2.11) and (2.12)), it is only suggestive that a quench method of solution will provide the correct ground state. In part, this is why we have carried out the extensive numerical comparisons reported in this work. The initial, trial wavefunction is of particular importance when the ASM is being carried out. Clearly, one wants to use the wavefunctions determined on a previous MD step as the initial wavefunction for the quench on the succeeding MD step. In the CcO TeDH-ASM simulation, with at most two active protons and the heavy-atom distances of 2.6–2.8 Å, a broad initial wavefunction was used and the number of quench iterations was fairly constant. The solvation bandwidth of ~5 kcal/mol indicates that, on any particular MD step, the solvated proton surface will be sufficiently asymmetric to well localize the proton. Such states are not challenging for the TeDH method.

The CcO simulation considered the oxygen–oxygen distances in the two waters–Glu286 cycle to be fixed. In a protein, these distances will fluctuate indicating that a vibrational force field for the oxygen–oxygen distances should be used. Because we find that our results are only

modestly dependent on these distances, introduction of these effects should not lead to substantial modifications. However, the motion of the waters after protonation is an important issue to address. The addition of the excess proton and the switch from the MD force field to the quantum treatment of the active protons changes the forces and may well lead to the cycle breaking up, or adding additional water molecules. Indeed, in order for proton translocation to proceed, such events must occur. That is why we did not attempt to formulate a rate constant for the protonation process. Clearly, protonation of a water/residue cycle, or other structures that form, must lead to new geometric configurations that can pass protons across the membrane.

Acknowledgement

The financial support of the National Institutes of Health (GM62790) is gratefully acknowledged. We are indebted to Professor S. Ferguson-Miller for providing the coordinates of *Rhodobacter sphaeroides* used in the simulation of CcO, to members of her group (Dr. D. Mills and Mr. B. Schmidt) and to Dr. S. Seibold for help in preparing the CcO input file, and to all of them for numerous enlightening discussions about CcO.

Appendix A. The time-dependent Hartree approximation to the Schrödinger equation for any of the degrees of freedom is

$$\mathrm{i}\hbar\frac{\partial\varphi(x,t)}{\partial t}=\hat{H}(x,t)\varphi(x,t). \tag{A.1}$$

We shall use the more conventional time version for this analysis and obtain the temperature version by the substitution, $t=-\mathrm{i}\beta\hbar$. As a reminder of the operator nature of the Hamiltonian, we use a ˆ on it. In contrast with the exact Schrödinger equation with its time-independent $\hat{H}$, the propagator $U(t,t_0)$ must be expressed as an ordered exponential

$$\begin{aligned}U(t,t_0)&=T_+\mathrm{e}^{-\mathrm{i}\int_{t_0}^{t}\mathrm{d}s\hat{H}(s)}\\&\equiv 1+(-\mathrm{i})\int_{t_0}^{t}\mathrm{d}s\hat{H}(s)+(-\mathrm{i})^2\int_{t_0}^{t}\mathrm{d}s_1\\&\quad\times\int_{t_0}^{s_1}\mathrm{d}_2\hat{H}(s_1)\hat{H}(s_2)+\cdots\end{aligned} \tag{A.2}$$

that is properly time ordered because $s_2<s_1$. The issue here is to assess the error made in using the Trotter formula in the form of the second-order, split-exponential operator formula. If the error is no worse than the $0(\Delta t)^3$ error of this split-operator formula for a time-*independent* Hamiltonian [79–82], then we anticipate that the method will be a fast and reliable method to obtain the ground-state wavefunction.

For the step from $t_0\to t_0+\Delta t$, we may write a second-order midstep expression,

$$\begin{aligned}\hat{H}(s)&\approx\hat{H}(t_0+\Delta t/2)+[s-(t_0+\Delta t/2)]\dot{\hat{H}}(t_0+\Delta t/2)\\&\quad+\frac{[s-(t_0+\Delta t/2)]^2}{2}\ddot{\hat{H}}(t_0+\Delta t/2)\end{aligned} \tag{A.3}$$

with $t_0<s<t_0+\Delta t$. Using this expression in Eq. (A.1) and evaluating all the terms shows that the error term is still of $0(\Delta t)^3$ and is the same error as for a time-independent $\hat{H}$. The non-commutativity arising from the time-dependent Hamiltonian, $[\hat{H}(s_1),\dot{\hat{H}}(s_2)]\neq 0$; $(s_1\neq s_2)$, does not contribute to the error to $0(\Delta t)^3$. Another approach is to expand about t_0 the beginning of the interval. When this is done, the error term is $\hat{H}(t_0)\dot{\hat{H}}(t_0)(\Delta t)^3$, and is of the same order as that of the time-independent, split-operator form. While a half-step formalism for the split-operator method can be developed, the overhead incurred in such a formula seems not to be worth the effort, because the error of the standard split-operator formula arising from the non-commutativity $[\hat{T},\hat{V}]\neq 0$ is of the same order as that incurred in the $\dot{\hat{H}}(t)$ case with expansion about t_0. Unless there was an unfavorable numerical coefficient that would significantly reduce its accuracy, the above error estimate indicates that the expansion about t_0 should be used, and we do so in this work. Thus, a working formula for a Hamiltonian schematized as $\hat{H}(t)=\hat{T}+V_0+\bar{V}(t)$, based on Eq. (A.1) and the above considerations is

$$\begin{aligned}\psi(t_0+\Delta t)&=T_+\mathrm{e}^{-(\mathrm{i}/\hbar)\int_{t_0}^{t_0+\Delta t}\mathrm{d}\hat{H}(s)}\psi(t_0)\\&\approx\mathrm{e}^{-(\mathrm{i}/\hbar)\hat{H}(t_0)\Delta t}\psi(t_0)\\&\approx\mathrm{e}^{-(\mathrm{i}/\hbar)\hat{T}\Delta t/2}\mathrm{e}^{-(\mathrm{i}/\hbar)(V_0+\bar{V}(t_0))\Delta t}\mathrm{e}^{-(\mathrm{i}/\hbar)\hat{T}\Delta t/2}\psi(t_0).\end{aligned} \tag{A.4}$$

As the wavefunction is known at time t_0, the expectation value $\bar{V}(t_0)$ is available to propagate to $t_0+\Delta t$. The substitution $t=-\mathrm{i}\beta\hbar$ then yields Eq. (2.13).

References

[1] D. Voet, J.G. Voet, Biochemistry, John Wiley & Sons, New York, 2004.
[2] J.F. Nagle, S. Tristam-Nagle, J. Membr. Biol. 74 (1983) 1.
[3] N. Agmon, Chem. Phys. Lett. 244 (1995) 456.
[4] R.A. Mathies, S.W. Lin, J.B. Ames, W.T. Pollard, Annu. Rev. Biophys. Chem. 20 (1991) 491.
[5] M.Y. Okamura, G. Feher, Annu. Rev. Biochem. 61 (1992) 861.
[6] L. Baciou, H. Michel, Biochemistry 34 (1995) 7967.
[7] S. Ferguson-Miller, G.T. Babcock, Chem. Rev. 96 (1996) 2889.
[8] M. Wikström, Bba-Bioenergetics 1458 (2000) 188.
[9] P. Brzezinski, G. Larsson, Bba-Bioenergetics 1605 (2003) 1.
[10] A. Warshel, J. Phys. Chem. 86 (1982) 2218.
[11] D. Borgis, G. Tarjus, H. Azzouz, J. Phys. Chem. 96 (1992) 3188.
[12] H. Azzouz, D. Borgis, J. Chem. Phys. 98 (1993) 7361.

[13] T.N. Truong, J.A. McCammon, D.J. Kouri, D.K. Hoffman, J. Chem. Phys. 96 (1992) 8136.
[14] P. Bala, B. Lesyng, J.A. McCammon, Chem. Phys. 180 (1994) 271.
[15] S. Hammes-Schiffer, J.C. Tully, J. Phys. Chem. 99 (1995) 5793.
[16] J.-Y. Fang, S. Hammes-Schiffer, J. Chem. Phys. 107 (1997) 5727.
[17] D. Laria, R. Kapral, D. Estrin, G. Ciccotti, J. Chem. Phys. 104 (1996) 6560.
[18] S. Consta, R. Kapral, J. Chem. Phys. 101 (1994) 10908.
[19] A. Staib, D. Borgis, J. Chem. Phys. 103 (1995) 2642.
[20] J. Mavri, H.J.C. Berendsen, W.Fv. Gunsteren, J. Phys. Chem. 97 (1993) 13469.
[21] D. VanDerSpoel, H.J.C. Berendsen, J. Phys. Chem. 100 (1996) 2535.
[22] J. Lobaugh, G.A. Voth, J. Chem. Phys. 104 (1996) 2056.
[23] M. Pavese, S. Chawla, D. Lu, J. Lobaugh, G.A. Voth, J. Chem. Phys. 107 (1997) 7428.
[24] K. Ando, J.T. Hynes, J. Phys. Chem. B 101 (1997) 10464.
[25] R.I. Cukier, J. Zhu, J. Phys. Chem. 101 (1997) 7180.
[26] R.I. Cukier, J. Zhu, J. Chem. Phys. 110 (1999) 9587.
[27] S. Hammes-Schiffer, S.R. Billeter, Int. Rev. Phys. Chem. 20 (2001) 591.
[28] M.L. Brewer, U.W. Schmitt, G.A. Voth, Biophys. J. 80 (2001) 1691.
[29] M.A. Lill, V. Helms, Proc. Natl. Acad. Sci. USA 99 (2002) 2778.
[30] R. Pomes, B. Roux, Biophys. J. 82 (2002) 2304.
[31] B. Roux, Acc. Chem. Res. 35 (2002) 366.
[32] G.A. Voth, Front. Biosci. 8 (2003) S1384.
[33] R. Pomes, C.H. Yu, Front. Biosci. 8 (2003) D1288.
[34] V. Zoete, M. Meuwly, J. Chem. Phys. 120 (2004) 7085.
[35] Y.J. Wu, G.A. Voth, Biophys. J. 85 (2003) 864.
[36] J. Lobaugh, G.A. Voth, J. Chem. Phys. 100 (1994) 3039.
[37] J.-K. Hwang, A. Warshel, J. Phys. Chem. 97 (1993) 10053.
[38] R. Pomès, B. Roux, J. Phys. Chem. 100 (1996) 2519.
[39] J. Cao, G.A. Voth, J. Chem. Phys. 99 (1993) 1070.
[40] J. Cao, G.A. Voth, J. Chem. Phys. 100 (1994) 5106.
[41] U.W. Schmitt, G.A. Voth, J. Chem. Phys. 111 (1999) 9361.
[42] Y. Ohta, K. Ohta, K. Kinugawa, Int. J. Quantum Chem. 95 (2003) 372.
[43] H. Decornez, K. Drukker, M.M. Hurley, S. Hammes-Schiffer, Ber. Bunsenges. Phys. Chem. 102 (1998) 533.
[44] A.B. McCoy, R.B. Gerber, M.A. Ratner, J. Chem. Phys. 101 (1994) 1975.
[45] N. Makri, W.H. Miller, J. Chem. Phys. 87 (1987) 5781.
[46] U. Manthe, H.-D. Meyer, L.S. Cederbaum, J. Chem. Phys. 97 (1992) 3199.
[47] F.A. Bornemann, P. Nattesheim, C. Schütte, J. Chem. Phys. 105 (1996) 1074.
[48] J. Wilkie, M.A. Ratner, R.B. Gerber, J. Chem. Phys. 110 (1999) 7610.
[49] H.D. Meyer, G.A. Worth, Theor. Chem. Acc. 109 (2003) 251.
[50] R. Pomès, B. Roux, Chem. Phys. Lett. 234 (1995) 416.
[51] J.-Y. Fang, S. Hammes-Schiffer, J. Chem. Phys. 106 (1997) 8442.
[52] S. Hammes-Schiffer, J. Chem. Phys. 105 (1996) 2236.
[53] K. Drukker, S. Hammes-Schiffer, J. Chem. Phys. 107 (1997) 363.
[54] K. Drukker, S.Wd. Leeuw, S. Hammes-Schiffer, J. Chem. Phys. 108 (1998) 6799.
[55] K. Laasonen, M. Sprik, M. Parrinello, R. Car, J. Chem. Phys. 99 (1993) 9081.
[56] M. Sprik, J. Hutter, M. Parrinello, J. Chem. Phys. 105 (1996) 1142.
[57] M.E. Tuckerman, K. Laasonen, M. Sprik, M. Parrinello, J. Chem. Phys. 103 (1995) 150.
[58] M.E. Tuckerman, K. Laasonen, M. Sprik, M. Parrinello, J. Phys. Chem. 99 (1995) 5749.
[59] D.E. Sagnella, K. Laasonen, M.L. Klein, Biophys. J. 71 (1996) 1172.
[60] H.S. Mei, M.E. Tuckerman, D.E. Sagnella, M.L. Klein, J. Phys. Chem. B 102 (1998) 10466.
[61] R. Car, M. Parrinello, Phys. Rev. Lett. 55 (1985) 2471.
[62] M.E. Tuckerman, J. Phys. Condens. Matter 14 (2002) R1297.
[63] R.P. Feynman, A. Hibbs, Quantum Mechanics and Path Integrals, McGraw-Hill, New York, 1965.
[64] A. Selloni, P. Carnevali, R. Car, M. Parrinello, Phys. Rev. Lett. 59 (1987) 823.
[65] R.N. Barnett, U. Landman, A. Nitzan, J. Chem. Phys. 89 (1988) 2242.
[66] P.J. Rossky, J. Schnitker, J. Phys. Chem. 92 (1988) 4277.
[67] S.-Y. Sheu, R.I. Cukier, J. Chem. Phys. 94 (1991) 8258.
[68] J. Zhu, R.I. Cukier, J. Chem. Phys. 98 (1993) 5679.
[69] P.A.M. Dirac, Proc. Camb. Philos. Soc. 26 (1930) 376.
[70] A.D. McLachlan, Mol. Phys. 8 (1963) 39.
[71] E.J. Heller, J. Chem. Phys. 64 (1976) 63.
[72] J. Frenkel, Wave Mechanics, Advanced General Theory, Clarendon Press, Oxford, 1934.
[73] D.J. Thouless, The Quantum Mechanics of Many-body Systems, Academic Press, New York, 1961.
[74] R.I. Cukier, Biochim. Biophys. Acta 1655 (2004) 37.
[75] R.I. Cukier, Biochim. Biophys. Acta 1656 (2004) 189.
[76] A. Puustinen, J.A. Bailey, R.B. Dyer, S.L. Mecklenburg, M. Wikstrom, W.H. Woodruff, Biochemistry 36 (1997) 13195.
[77] P.R. Rich, J. Breton, S. Junemann, P. Heathcote, Bba-Bioenergetics 1459 (2000) 475.
[78] D. Heitbrink, H. Sigurdson, C. Bolwien, P. Brzezinski, J. Heberle, Biophys. J. 82 (2002) 1.
[79] M.D. Feit, J.J.A. Fleck, A. Steiger, J. Comput. Phys. 47 (1982) 412.
[80] M.D. Feit, J.J.A. Fleck, J. Chem. Phys 78 (1983) 301.
[81] M.D. Feit, J.J.A. Fleck, J. Chem. Phys. 80 (1984) 2578.
[82] R. Kosloff, J. Phys. Chem. 92 (1988) 2087.
[83] X. Duan, S. Scheiner, J. Mol. Struct. 270 (1992) 173.
[84] S. Scheiner, X. Duan, in: D.A. Smith (Ed.), Modelling the Hydrogen Bond, ACS Symposium Series, Washington, DC, 1994, p. 125.
[85] R.I. Cukier, S.A. Seibold, J. Phys. Chem. B 16 (2002) 12031.
[86] W.F. van Gunsteren, H.J.C. Berendsen, GROMOS Manual, University of Groningen, Groningen, 1987.
[87] R.W. Hockney, J.W. Eastwood, Computer Simulation Using Particles, McGraw-Hill, New York, 1981.
[88] M.P. Allen, D.J. Tildesley, Computer Simulation of Liquids, Clarendon Press, Oxford, 1987.
[89] J.P. Ryckaert, G. Ciccotti, H.J.C. Berendsen, J. Comput. Phys. 23 (1977) 327.
[90] H.H.C. Berendsen, J.P.M. Postma, W.F. Gunsteren, A. DiNola, J.R. Haak, J. Chem. Phys. 81 (1984) 3684.
[91] M. Svensson-Ek, J. Abramson, G. Larsson, S. Tornroth, P. Brzezinski, S. Iwata, J. Mol. Biol. 321 (2002) 329.
[92] H. Hellmann, Einfuhrung in die Quantumchemie, Franz Deuticke, Leipzig, 1937.
[93] R.P. Feynman, Phys. Rev. 56 (1939) 340.
[94] W.R. Forsyth, J.M. Antosiewiez, A.D. Robertson, Proteins 48 (2002) 388.
[95] J.J. Dwyer, A.G. Gittis, D.A. karp, E.E. Lattman, D.S. Spencer, W.E. Stites, E. BG-M, Biophys. J. 79 (2000) 1610.
[96] M.J. Frisch, G.W. Trucks, H.B. Schlegel, G.E. Scuseria, M.A. Robb, J.R. Cheeseman, V.G. Zakrzewski, J.A. Montgomery Jr., R.E. Stratmann, J.C. Burant, S. Dapprich, J.M. Millam, A.D. Daniels, K.N. Kudin, M.C. Strain, O. Farkas, J. Tomasi, V. Barone, M. Cossi, R. Cammi, B. Mennucci, C. Pomelli, C. Adamo, S. Clifford, J. Ochterski, G.A. Petersson, P.Y. Ayala, Q. Cui, K. Morokuma, P. Salvador, J.J. Dannenberg, D.K. Malick, A.D. Rabuck, K. Raghavachari, J.B. Foresman, J. Cioslowski, J.V. Ortiz, A.G. Baboul, B.B. Stefanov, G. Liu, A. Liashenko, P. Piskorz, I. Komaromi, R. Gomperts, R.L.

Martin, D.J. Fox, T. Keith, M.A. Al-Laham, C.Y. Peng, A. Nanayakkara, M. Challacombe, P.M.W. Gill, B. Johnson, W. Chen, M.W. Wong, J.L. Andres, C. Gonzalez, M. Head-Gordon, E.S. Replogle, J.A. Pople, Gaussian 98, Gaussian Inc., Pittsburgh, PA, 2001.
[97] P. Adelroth, M. Karpefors, G. Gilderson, F.L. Tomson, R.B. Gennis, P. Brzezinski, Biochim. Biophys. Acta 1459 (2000) 533.
[98] B. Meunier, C. Ortwein, U. Brandt, P.R. Rich, Biochem. J. 330 (1998) 1197.
[99] B. Rost, J. Behr, P. Hellwig, O.M.H. Richter, B. Ludwig, H. Michel, W. Mantele, Biochemistry 38 (1999) 7565.
[100] S. Junemann, B. Meunier, N. Fisher, P.R. Rich, Biochemistry 38 (1999) 5248.
[101] C. Backgren, G. Hummer, M. Wikstrom, A. Puustinen, Biochemistry 39 (2000) 7863.
[102] A. Aagaard, G. Gilderson, D.A. Mills, S. Ferguson-Miller, P. Brzezinski, Biochemistry 39 (2000) 15847.
[103] A.A. Stuchebrukhov, J. Theor. Comp. Chem. 2 (2003) 91.